ISSN 1027-5495. Functional Materials, 22, No.4 (2015), p. 487-493.
doi:http://dx.doi.org/10.15407/fm22.04.487

Effect of substrate temperature on structural and substructural properties of MgO thin films

***O.V.Diachenko*[1,3], *A.S.Opanasuyk*[1], *D.I.Kurbatov*[1], *V.M.Kuznetsov*[2], *H.Cheong*[3]**

[1]Sumy State University, 2 Rymsky-Korsakov Str., 40007 Sumy, Ukraine
[2]Institute of Applied Physics, National Academy of Sciences of Ukraine, 58 Petropavliska Str., 40030 Sumy, Ukraine
[3]Department of Physics, Sogang University, Seoul 121-742, South Korea

Received April 4, 2015

In this paper we have studied the influence of substrate temperature deposition on structural and substructural characteristics of magnesium oxide films by X-ray diffraction analysis. The thin films of MgO were prepared by spray pyrolysis technique from magnesium chloride solution. We have established the phase composition, the lattice constant, coherent scattering domain size, microstrain level of the films. The optimal conditions for the application of the homogeneous single-phase films of stoichiometric composition were identified.

Keywords: magnesium oxide, spray pyrolysis technique, X-ray diffraction analysis, substructural characteristics, coherent scattering domain size, microstrain.

Методом рентгенодифракционного анализа проведено исследование влияния температуры подложки при осаждении на структурные и субструктурные характеристики пленок оксида магния. Пленки получены методом спрей-пиролиза из раствора хлорида магния. Определены фазовый состав, период кристаллической решетки, размер областей когерентного рассеяния, уровень микродеформаций в пленках, полученных при различных температурах осаждения. Установлены оптимальные условия нанесения однородных однофазных пленок стехиометрического состава.

Вплив температури підкладки на структурні та субструктурні характеристики тонких плівок MgO. *О.В.Д'яченко, А.С.Опанасюк, Д.І.Курбатов, В.М.Кузнецов, Х.Чеонг.*
Методом рентгенодифракційного аналізу проведено дослідження впливу температури підкладки під час осадження на структурні та субструктурні характеристики плівок оксиду магнію. Плівки отримано методом спрей-піролізу з розчину хлориду магнію. Визначено фазовий склад, період кристалічної гратки, розмір областей когерентного розсіювання, рівень мікродеформацій у плівках, отриманих при різних температурах осадження. Встановлено оптимальні умови нанесення однорідних однофазних плівок стехіометричного складу.

1. Introduction

Magnesium oxide (MgO) is broad-gap semiconductor compound, which due to its physical and chemical properties has wide practical application. Single-crystal MgO films are widely used as chemically stable substrate for growing high-temperature superconductors and ferroelectric materials [1–4], as dielectric layer of plasma screens [5, 6], as insulator, alternative to SiO_2, for use in high capacity electrical circuits [7], etc. In addition, this compound has been used as antireflection layer in solar cells and as a gate in MOSFETs etc. [8].

MgO relates to II–VI group wide-gap semiconductors which have attracted much attention of researchers due to their unique electrical and optical properties [9]. It has the crystalline structure similar to NaCl and characterized by wide band gap (E_g = 7.3 eV), high thermal conductivity and melting temperature of 3125 K [5, 7, 8, 10, 11].

There are different methods to obtain the MgO thin films and nanostructures of such as: pulsed laser and thermal evaporation, high frequency magnetron sputtering cathode, chemical vapor deposition, spray pyrolysis [10, 12–16], etc. Lately, non-vacuum methods, among them spray pyrolysis, was also used for deposition of metal oxides. This method is one of the most promising for semiconductors film deposition and insulators due to its low cost, high deposition rate and eligibility for deposition of large area thin films of different materials.

The majority of authors have studied structural, electrical and optical properties of the MgO films, deposited by the spray pyrolysis technique, using precursors based on magnesium acetate or magnesium acetylacetonate [16–21]. The presented paper describes the results of comprehensive study of the influence of deposition temperature on the structural and substructural properties of thin films obtained from magnesium chloride solution.

2. Experimental

Magnesium oxide films were obtained on glass substrates 1×1 cm^2 by spray pyrolysis technique. Before deposition the substrates surface were cleaned in ultrasonic bath for 8 min. We used 0.2 M magnesium chloride hexahydrate ($MgCl_2 \cdot 6H_2O$) aqueous solution as precursor solution.

Previous experimental studies [1], allowed to determine temperature conditions for obtaining the single-phase magnesium oxide films. Thus, obtaining of the films was carried out at the substrate temperature range of T_s = 640 K to 690 K with step Δ10 K. For synthesis of the thin layers we used the setup described in the papers [2, 22].

Substrates temperature during the films obtaining was measured using a chromel-alumel thermocouple. Distance between the nozzle and the heated substrate was equal to 12 cm. To transport the dispersed precursor particles, air flow with pressure of 0.25 MPa was used. Spraying rate was 2 ml/min at volume of the sprayed solution of 2 ml per the sample.

Automated X-ray diffractometer DRON 4-07 was used to determine the structural properties. All measurements were carried out in Ni-filtered Kα radiation of copper anode (U = 30 kV, I = 20 mA) in the range of 2θ angles from 20° to 80°, where 2θ is the Bragg's angle in continuous registration mode (speed — 1°/min, 0.02 degrees step). Experimental results were transferred directly into DifWin software for the experimental data analysis. Accuracy of determination of the lattice constant of the material was 0.001 % [25].

The diffraction patterns were normalized to the peak intensity of (200) plane cubic phase of the compound. Phase analysis was performed by comparing the interplane distances and relative intensities of the investigated samples and the standard according to JCPDS [23].

The texture quality of the films has been estimated by the Harris method [9, 22, 24–26]. Pole density was calculated by the following formula:

$$P_i = \frac{(I_i / I_{0i})}{1/N \sum_{i=1}^{N} (I_i / I_{0i})},$$

where I_i, I_{0i} are integrated intensities of i-th diffraction peak for the film sample and standard; N is number of lines that are present on the diffraction pattern.

After that P_i — $(hkl)_i$ and P_i — φ dependences were plotted, where φ is the angle between the axis of the texture and perpendicular to different crystallographic planes, which correspond to the reflections in the XRD patterns, (hkl) — Miller indexes. This angle was calculated for the cubic lattice, using the expressions given in [25]. Texture axis has those indexes, which correspond to the largest value of P_i.

The orientation factor of the sample can be calculated from the expression:

$$f = \sqrt{\frac{1}{N} \sum_{i=1}^{N} (P_i - 1)^2} \quad .$$

Calculation of constants a of the cubic phase of the material was performed sing the following formula [26]:

$$a = \frac{\lambda}{2\sin\theta} \sqrt{(h^2 + k^2 + l^2)}.$$

The lattice constants were determined using the Nelson-Riley extrapolation

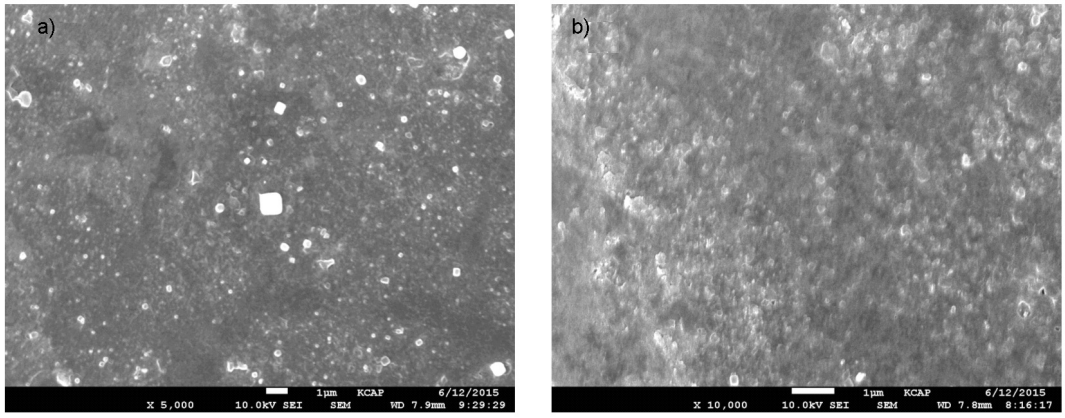

Fig. 1. Images of surface of films obtained at T_s, K: 660 (a) and 690 (b).

method [22, 25]. The linear approximation of obtained points was carried out using the method of least squares with the help of OriginPro software package.

The diffractometrical method was also used for estimation of average values of coherent scattering domain size (CSD) L and microstrain (ε) according to half-width of the diffraction lines. To separate the diffraction broadening caused by physical and instrumental effects we used approximations of the X-ray line by the Cauchy and Gauss functions. Further separation of the contributions from dispersion on CSD and microstrain was performed by the Williamson-Hall graphical method. Namely, the experimental data were presented in $\beta\cos\theta/\lambda$ $-4\sin\theta/\lambda$ and $(\beta\cos\theta/\lambda)^2$ $-(4\sin\theta/\lambda)^2$ coordinates, where β is physical broadening of X-ray line, λ is X-rays wavelength [21]. Additionally, the microstrain and size of CSD were determined by the method of approximation of the X-ray line as threefold convolution [25]:

$$L = \lambda / \cos\theta_1 \cdot \frac{tB_1 - cB_2}{t\beta_{f1}^2 - \beta_{f2}^2},$$

$$\varepsilon^2 = \frac{c\beta_{f1}^2 B_2 - \beta_{f2}^2 B_1}{16\mathrm{tg}\theta_1 (cB_2 - tB_1)},$$

where $t = \mathrm{tg}^2\theta_2/\mathrm{tg}^2\theta_1$; $c = \cos\theta_1/\cos\theta_2$; $\beta_{fi} = \sqrt{(B_i)^2 - (b_i)^2}$; θ_1 and θ_2 — are diffraction angles of the pairs of analyzed lines; and B_i, b_i, β_{fi} are the measured, instrumental and physical broadening of the corresponding X-ray lines.

The microstresses level was calculated by the formula $\sigma = E\varepsilon$ where E is the Young's modulus, which equal to $E = 90$ GPa and it was taken from [27].

Further using the CSD size values and microstrains the average dislocation density within CSD, on their boundaries, and its total value was estimated. In this case, we used the following equations. The average dislocation density, which forms the boundaries of the blocks, is $\rho_L = 3n/L^2$ [26], where n is number of the dislocations in each of six faces of the block. If the dislocations are located mainly inside CSD, the dislocation density is calculated by $\rho_\varepsilon = 4/F(2\varepsilon/d_0)^2$ [26], where F shows how many times the dislocation energy grows under interaction with other dislocations; and d_0 is the lattice constant of the material in appropriate direction. Taking $n = F = 1$, the minimal value of ρ_L and maximal value for ρ_ε can be estimated. To determine the total concentration of the dislocations we used another equation $\rho = 15\varepsilon/(d_0 L)$ [25]. These allowed us to calculate the dislocations concentration, in the within CSD, on their boundaries, and the total concentration.

3. Results and discussion

Using scanning electron microscope (SEM) the films surface was investigated. SEM images of magnesium oxide films (Fig. 1) showed that the films contain with amorphous phase as well as crystallites mostly with cubic shape.

Fig. 2a shows the diffraction patterns of the MgO films deposited at substrate temperatures from $T_s = 640$ to 690 K. The analysis showed that all XRD lines corresponding to the cubic phase of MgO. Reflection from crystallographic planes of other phases was not observed in the diffraction

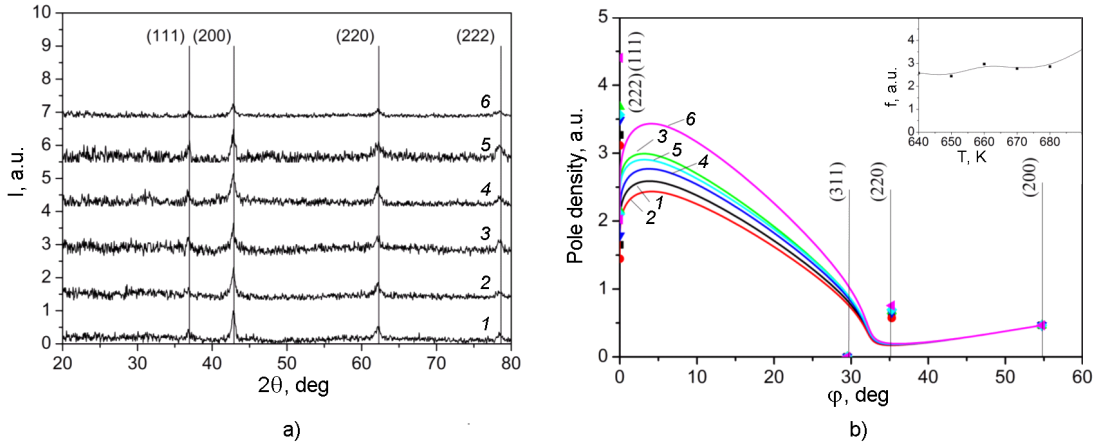

Fig. 2. XRD patterns (a) and pole density (P_i) as dependent function of angle φ between axis of the texture and normal to the reflecting plane (b) of MgO films obtained at T_s, K: 640 (*1*), 650 (*2*), 660 (*3*), 670 (*4*), 680 (*5*) and 690 (*6*) and orientation factor (*f*) for the films obtained at different substrate temperatures (inset).

patterns. It was indicated that in this temperature range, the obtained samples were single-phase (according to accuracy of the method). It should be noted that magnesium hydroxy compounds were observed in the films obtained at substrate temperatures $T_s < 640$ K [2].

X-ray analysis showed that reflections from crystallographic planes of (111) and (200) of cubic phase of magnesium oxide had the dominant intensity, which indicated the growth texture in the films.

Calculations of the pole density P_i and orientation factor f confirmed presence of pronounced axial growth texture of MgO layers [111]. Fig. 2b shows that similar growth texture was also observed by the other researchers, in [20, 21, 28].

Fig. 2b (inset) shows the dependences orientation factor on the substrate temperature. As can be seen from the figure, with increasing the substrate temperature, the texture quality also increases.

The dependence of the lattice constant of MgO on the substrate temperature is presented in Fig. 3. The dotted line in the figure shows the reference values given for this compound [23].

As can be seen from the figure, the lattice constant of MgO layer that was obtained at $T_s = 640$ K is equal to $a = 0.42154$ nm. These values are lower than the reference ones. With increasing the substrate temperature we observed a gradual increase in the lattice constant of the material ($a = 0.42270$ nm at $T_s = 660$ K) to values that exceed the reference ($a = 0.42270$ nm [23]).

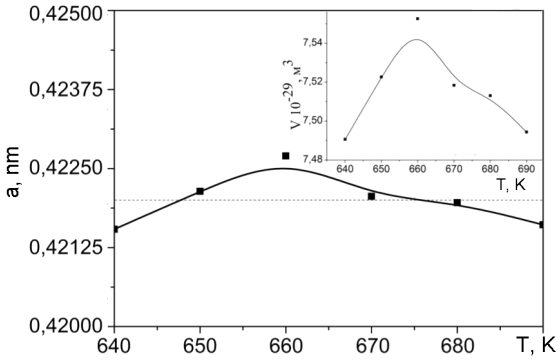

Fig. 3. Dependence of lattice constant of MgO on substrate temperature and volume of primitive cubic cell in the obtained MgO films (inset).

With the further increase of T_s the lattice parameter of MgO decreased.

Further, using calculated values of the lattice constant the volume of a primitive cubic cell was found. As could be seen from Fig. 3, (inset) the increasing of the substrate temperature from $T_s = 640$ K to $T_s = 660$ K led to increase of the cell volume from $V = 74.91 \cdot 10^{30}$ m^{-3} to $V = 75.53 \cdot 10^{30}$ m^{-3}. With the further increase of T_s the volume of the primitive cubic cell is decrease to $V = 74.94 \cdot 10^{30}$ m^{-3}, while reference data of V are equal to $75.15 \cdot 10^{30}$ m^{-3}.

Estimations of the substructural parameters of the obtained films were carried out for [111] direction of crystal lattice of the cubic phase (by reflections from (100) plane and (222) plane). The results of calculations of the CSD and microstrain are summarized in Table 1 and Fig. 4. As can be seen from

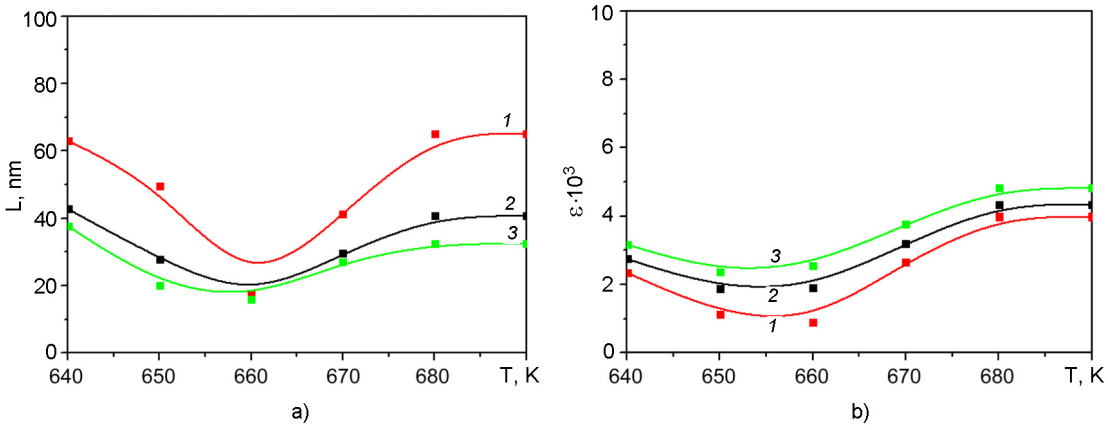

Fig. 4. Effect of substrate temperature on (a) CSD L and (b) microstrain e obtained using the Gauss (*1*) and Cauchi (*3*) approximation and from threefold convolution (*2*).

Fig. 4, the values of the substructural parameters, obtained with the help of different approximations, correlate well with each other, as it should be on theoretical considerations. This confirms the reliability of the results. However, the most accurate values were obtained by threefold convolution of the functions.

It is shown (Fig. 4a) that increasing the substrate temperature of the thin films leads to decrease of CSD from L ~ 43 nm (T_s = 640 K) to L ~ 16 nm (T_s = 660 K) in the [111] direction and then increase to L ~ 41 nm (T_s = 690 K). The authors of [19] using the Sherrer's ratio obtained similar values of the CSD sizes (L = 15 nm) for magnesium oxide films obtained at temperatures of 673 K and 723 K from solutions of magnesium acetylacetonate as precursor. Also, similar results L = 16 nm were obtained in [17]. These authors have synthesized films at temperature range from T_s = 673 K to 873 K using magnesium acetate as precursor in ethanol with HCl and TEG.

Fig. 4b shows that the dependence of microstrains level on growth temperature has the similar trend as the CSD dependences. Firstly the microstrains of thin films decrease from $2.75 \cdot 10^{-3}$ (T_s = 640 K) to $1.89 \cdot 10^{-3}$ (T_s = 650 K) and then increase to $4.35 \cdot 10^{-3}$ (T_s = 690 K).

The estimations of the microstrain allowed to calculate microstress (σ) in the films, and it was established that the microstress values varied in the range of σ = 172–392 MPa.

On the basis of the substructure calculations the average dislocation density in the films was estimated (Table 2). It well known that in II–VI compounds the dislocations are active recombination centers that limit the lifetime of the free charge carriers. Figure 5 shows the average dislocation density at the boundaries of CSD, in the bulk and the total dislocation density as function of the substrate temperature. As can be seen from the Fig. 5, with increasing of the substrate temperature we observed some increase in the average dislocation density at

Table 1. Sub-structural features of MgO films obtained using different approximations

T, K	(*hkl*)	L, nm			ε·10³		
		Approximation by		From convolution	Approximation by		From convolution
		Gauss	Cauchi		Gauss	Cauchi	
640	(111)–(222)	37.7	63.1	42.8	3.17	2.35	2.75
650	(111)–(222)	20.1	49.5	27.9	2.37	1.14	1.89
660	(111)–(222)	16.1	17.8	16.2	2.56	0.91	1.91
670	(111)–(222)	27.2	41.4	29.6	3.77	2.67	3.19
680	(111)–(222)	32.5	65.2	40.7	4.82	3.99	4.35
690	(111)–(222)	32.5	65.2	40.7	4.82	3.99	4.35

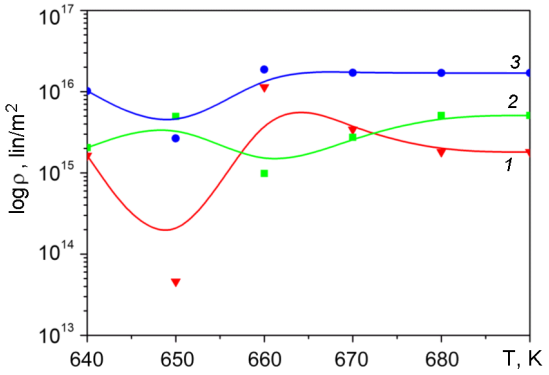

Fig. 5. Dependences of dislocation density on substrate temperature: (*1*) dislocations located mainly in the bulk of CSD; (*2*) dislocations that form the boundaries of the blocks; (*3*) the total concentration of dislocations in the material.

the boundaries of CSD and then its decrease. Whereas, the concentration of the dislocations on the boundary of CSD is slightly increase. As a result, the total dislocation density is almost independent of substrate temperature ($\rho_{L\varepsilon} = 1.02–1.87 \cdot 10^{-16}$ lin/m^2). The calculations indicate that the dislocations are mainly concentrated on the boundaries of CSD. The bulk of crystallites in the thin films are almost free from the dislocations.

4. Conclusions

In this paper we report the comprehensive study of the structural (texture quality and lattice constants) and sub-structural (coherent scattering domain size, microstrains, and dislocation density) characteristics of nanostructured magnesium oxide films obtained by spray pyrolysis technique at the different substrate temperatures. 0.2 M magnesium chloride hexahydrate ($MgCl_2 \cdot 6H_2O$) aqueous solution was used as precursor solution.

The X-ray diffractometric researches have allowed us to establish, that the MgO film were single-phase (according to accuracy of the method) and had cubic structure with the high-quality texture growth of [111], the quality of which depended on T_s. The values of lattice constant (a = 0.4215–0.4227 nm) were calculated. It was found the trend to the slight increase of a at the temperature of T_s = 640–660 K, with following decreasing of the lattice constant at the high temperatures.

It was established that the CSD sizes in the MgO films and microstrains in directions perpendicular to the crystallographic planes of (111) were $L_{(111)}$ = 16.2–42.8 nm and $\varepsilon \sim (1.89–4.35) \cdot 10^{-3}$, respectively.

On the basis of the calculations of ε and L, the average density of dislocations located in the bulk ($\rho_\varepsilon = 2.04–9.84 \cdot 10^{15}$ lin/m^2) and on the boundaries of CSD ($\rho_L = 1.14–3.85 \cdot 10^{-15}$ lin/m^2) and the total concentration ($\rho_{L\varepsilon} = 1.02–1.87 \cdot 10^{16}$ lin/m^2) of the dislocations were estimated.

It is shown that the MgO films with controlled structural properties can be obtained by changing the substrate temperature.

Acknowledgments. This research was supported by the Ministry of Education and Science of Ukraine (Grants No. 0113U000131 and No. 0112U000772).

References

1. W.B.Wang, Y.Yang, A.Yanguas-Gil et al., *Appl. Phys. Lett.*, **102**, 101605 (2013).
2. A.V.Dyachenko, A.S.Opanasuyk, D.I.Kurbatov et al., in: Proc. Intern. Conf. Nanomaterials: Applications and Properties 3, 01001 (2014).
3. S.S.P.Parkin, C.Kaiser, A.Panchula et al., *Nat. Mater.*, **3**, 862 (2004).
4. S.Ikeda, K.Miura, H.Yamamoto et al., *Nat. Mater.*, **9**, 721 (2010).
5. Y.B.Li, Y.Bando, T.Sato, *Chem. Phys. Lett.*, **359**, 141 (2002).
6. E.Fujiia, A.Tomozawaa et al., *Thin Solid Films*, **352**, 85 (1999).
7. J.Kim, B.P.Gila, R.Mehandru et al., in: Proc. Res. Soc. Symposium (2002), p.690.

Table 2. Structure and substructure properties of MgO thin films

T, K	a, nm	$V \cdot 10^{-29}$, m^3	σ, MPa	$\rho_L \cdot 10^{-15}$, lin/m^2	$\rho_\varepsilon \cdot 10^{-15}$, lin/m^2	$\rho_{L\varepsilon} \cdot 10^{-16}$, lin/m^2
640	0.42154	7.491	248	1.63	2.04	1.02
650	0.42214	7.523	386	3.85	9.47	1.07
660	0.42270	7.553	172	1.14	9.84	1.87
670	0.42206	7.518	288	3.41	2.75	1.71
680	0.42196	7.513	392	1.81	5.09	1.70
690	0.42161	7.494	392	1.81	5.09	1.70

8. Y.Peidong, C.M.Lieber, *Science*, **273**, 1836 (1996).
9. C.J.Panchal, A.S.Opanasyuk, V.V.Kosyak et al., *J. Nano-Electron. Phys.*, **3(1)**, 274 (2011).
10. M.Li, X.Wang, H.Li et al., *Appl. Surf. Sci.*, **274**, 188 (2013).
11. K.Hayashi, S.Matsuishi, T.Kamiya et al., *Nature*, **419**, 462 (2002).
12. J.Senzaki, K.Kurihara et al., *J. Appl. Phys.*, **37**, 5150 (1998).
13. M.Nashimoto, K.Nashimoto, *J. Appl. Phys.*, **33**, L793 (1994).
14. D.K.Fork, F.A.Ponce et al., *Appl. Phys. Lett.*, **58**, 2294 (1991).
15. S.K.Ram, U.K.Barik, S.Sarkar et al., *Thin Solid Films*, **517**, 6252 (2009).
16. O.Stryckmans, T.Segato, P.H.Duvigneaud, *Thin Solid Films*, **283**, 17 (1996).
17. A.Moses Ezhil Raj, L.C.Nehru, M.Jayachandran, C.Sanjeeviraja, *Cryst. Res. Technol.*, **42**, 867 (2007).
18. J.M.Bian, X.M.Li, T.L.Chen et al., *Appl. Surf. Sci.*, **228**, 297 (2004).
19. X.Fu, G.Wu, S.Song et al., *Appl. Surf. Sci.*, **148**, 223 (1999).
20. X.Yi, W.Wenzhong, Q.Yitai et al., *Surf. Coat. Techn.*, **82**, 291 (1996).
21. S.G.Kim, J.Y.Kim, H.J.Kim, *Thin Solid Films*, **376**, 110 (2000).
22. O.Dobrozhan, D.Kurbatov, A.Opanasyuk et al., *Surf. Interface Anal.*, **47**, 601 (2015).
23. Selected Powder Diffraction Data for Education Straining. Search Manual and Data Cards, USA: International Centre for Diffraction Data (1997).
24. D.Kurbatov, V.Kosyak, M.Kolesnyk et al., *Integrated Ferroelectrics*, **103**, 1 (2009).
25. Ja.S.Umanskij, Ju.A.Skakov, A.N.Ivanov, L.N.Rastorgujev, Crystallogaphy, X-ray Graph and Electronmicroscopy, Moscow (1982) (in Russian).
26. B.E.Warren, X-ray Diffraction, Dover, New York (1990).
27. W.J.De Sisto, R.L.Henry, *J. Cryst. Growth*, **109**, 314 (1991).
28. O.Yeheskel, R.Chaim, Z.Shen, M.Nygren, *J. Mater. Res.*, **20**, 719 (2005).